

# Large-scale maximal entanglement and Majorana bound states in coupled circuit quantum electrodynamic systems

Myung-Joong Hwang<sup>1</sup> and Mahn-Soo Choi<sup>2,3,\*</sup>

<sup>1</sup>*Department of Physics, Pohang University of Science and Technology, Pohang 790-784, Korea*

<sup>2</sup>*Department of Physics, Korea University, Seoul 136-713, Korea*

<sup>3</sup>*School of Physics, Korea Institute for Advanced Study, Seoul 130-722, Korea*

(Received 4 July 2012; published 7 March 2013)

We study the effect of ultrastrong cavity-qubit coupling on the low-lying excitations of a chain of coupled circuit quantum electrodynamic (QED) systems. We show that, in the presence of the onsite ultrastrong coupling, the photon hopping between cavities can be mapped to the Ising interaction between the lowest two levels of individual circuit QED of the chain. Based on our mapping, we predict two nearly degenerate ground states whose wave functions involve maximal entanglement between the macroscopic quantum states of the cavities and the states of qubits and identify that they are mathematically equivalent to Majorana bound states. Further, we devise a scheme for the dispersive measurement of the ground states using an additional resonator attached to one end of the circuit QED chain. Finally, we discuss the effects of disorders and local noises on the coherence of the ground states.

DOI: [10.1103/PhysRevB.87.125404](https://doi.org/10.1103/PhysRevB.87.125404)

PACS number(s): 73.21.-b, 42.50.-p

## I. INTRODUCTION

Confronted with formidable difficulties in solving strongly interacting many-body systems, it has been desired to find good quantum simulators. It may seem natural to simulate a many-body system with another tunable system of massive particles such as ultracold atomic gases.<sup>1</sup> In fact, any controllable quantum system, notably quantum computer if ever practical, can simulate efficiently many-body systems.<sup>2</sup> Indeed, it has been recognized that arrays of coupled photonic cavities, each coupled to a two-level system, can simulate closely the quantum behaviors of strongly correlated many-body systems.<sup>3-5</sup> Subsequent studies have revealed that the Bose-Hubbard model,<sup>6</sup> interacting spin models,<sup>5,7</sup> and other exotic quantum phases<sup>8</sup> can be simulated efficiently using the coupled cavities. Further, recent advances in solid-state devices such as circuit quantum electrodynamics (QED) systems<sup>9,10</sup> and microcavities<sup>11,12</sup> and ongoing efforts to fabricate large-scale cavity arrays<sup>13,14</sup> make the array of coupled cavities a promising candidate for an efficient quantum simulator.

The strongly interacting photons or polariton physics in the coupled cavities arise from the interplay between the onsite cavity-qubit coupling and the photon hopping between cavities. The onsite cavity-qubit coupling gives rise to a nonlinearity in the system and induces an effective onsite photon-photon interaction. While the cavity-qubit coupling rate is considered to be larger than the rates that the system loses its energy to the environment, the previous works have assumed that the cavity-qubit coupling rate is still much smaller than the cavity frequency and the transition frequency of the qubit. In this sense, studies on the coupled cavities have been limited to Jaynes-Cummings lattices model.<sup>15</sup>

Meanwhile, for a single cavity coupled to a single qubit, the so-called ultrastrong coupling has been envisioned<sup>16</sup> and experimentally demonstrated.<sup>17</sup> That is, the qubit-cavity coupling rate is comparable to or even higher than the cavity frequency. In the ultrastrong-coupling regime, processes that excite or deexcite the cavity and the qubit simultaneously, the so-called counter-rotating terms, can not be neglected and they

bring about fundamentally different physics deeply connected to the high degree of entanglement between the qubit and the photon.<sup>18-22</sup>

The main motivation of this paper is to investigate effects of the ultrastrong coupling on the low-lying excitations of the coupled cavities, thus exploring physics beyond the Jaynes-Cummings lattices. Although our discussion is not limited to a particular implementation of the coupled cavities, we mainly focus on the one-dimensional (1D) array of circuit QED systems (cQEDs), with each cQED being in the ultrastrong-coupling regime (see Fig. 1). An important finding of this paper is that, in the presence of the ultrastrong coupling, the photon hopping can be mapped to the Ising interaction between the effective spins that correspond to the lowest two levels of each cavity QED. With the energy splitting between the two levels playing the role of the Zeeman field for the effective spins, the cQED arrays realize a transverse-field Ising model. Interestingly, we find that while the transverse field decreases exponentially as a function of the ratio between the coupling strength and the cavity frequency, the Ising interaction strength increases quadratically. That is, the ultrastrong coupling drives the arrays to the magnetically ordered phase.

From our mapping, we find that the ultrastrong coupling leads to two nearly degenerate ground states separated by a finite-energy gap from the continuum of higher-energy states. We obtain an analytical expression for the ground states and find that the ground states are a superposition of two amplitudes: For one amplitude, each of the cavity fields is displaced to the  $+x$  direction in the phase space with an amplitude determined by the coupling strength, while each of the qubits is directing the  $+x$  direction in the Bloch sphere. For the other amplitude, all the cavities are displaced to the  $-x$  direction, while qubits are directing the  $-x$  direction. This is a truly large-scale qubit-cavity entanglement in that it involves macroscopic quantum states of the cavities in the entire chain and the states of the qubits.

Moreover, the interacting spin system realized in the ultrastrong-coupling regime can be mapped to the chain of

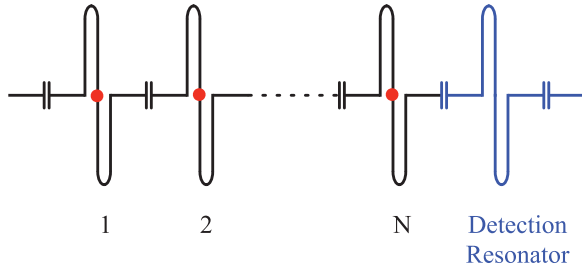


FIG. 1. (Color online) Schematic of 1D circuit QED arrays. The black lines represent the superconducting microwave resonators with a resonant frequency  $\omega_0$ , which are capacitively coupled to each other allowing photon hopping between resonators with an amplitude  $J$ . Each of the microwave resonators, labeled from 1 to  $N$ , contains a superconducting qubit (red dot), thus realizing a circuit QED with a cavity-qubit coupling strength  $\lambda$ . Particularly, the coupling strength  $\lambda$  is larger than the cavity photon frequency  $\omega_0$ , so that each of the circuit QEDs is in the ultrastrong-coupling regime.

Majorana fermions using the Jordan-Wigner transformation. Then, the magnetically ordered phase corresponds to the topologically nontrivial phase which supports Majorana bound states. Therefore, the circuit QED arrays with the ultrastrong coupling can be used to simulate this exotic physics.<sup>23</sup> Although the Majorana zero mode realized in this system does not inherit the topological protection against “real-space” local noises, the structure of the ground-state wave functions allows a partial protection from certain local noises. We show that the local fluctuation of qubits along the  $y$  and  $z$  directions (the ground states involve states of qubits directing  $\pm x$  directions in the Bloch sphere) can only come as a second-order effect. Moreover, we find that the decoherence rate is proportional to the relaxation rate of the individual qubit and it scales as the number of cQEDs in the array.

Finally, we suggest a scheme to probe the macroscopic ground states of the cQED arrays. By simply adding an additional cavity capacitively coupled to the one end of the array, the macroscopic ground states as a two-level system couple to the additional cavity field, thus realizing a standard Jaynes-Cummings Hamiltonian. Moreover, we show that the coupling strength between the additional cavity field and the ground states exceeds the decoherence rate of the ground states, thus realizing the strong-coupling regime. This allows a dispersive measurement of the ground states using the additional cavity and opens up a possibility to probe the Majorana bound state simulated in the circuit QED arrays.

The paper is organized as follows. In Sec. II A, we introduce the model for the cQED arrays. The single cQED Hamiltonian in the ultrastrong-coupling regime is analyzed in Sec. II B. The mapping of the photon hopping Hamiltonian to the Ising interaction Hamiltonian is established in Sec. II C, followed by the effective spin model for the cQED arrays in Sec. II D. From this effective model, the ground states of the cQED arrays in the ultrastrong-coupling regime are derived in Sec. II E. In Sec. III, we describe the system in terms of Majorana fermions and find that the ground states of the arrays correspond to the Majorana bound state. In Sec. IV, we derive the master equation and discuss the effects of noises. The effects of

disorder are also discussed. The detection scheme is proposed in Sec. V. We conclude our paper in Sec. VI with discussion of the experimental feasibility.

## II. ARRAY OF CIRCUIT QED SYSTEMS WITH THE ONSITE ULTRASTRONG COUPLING

### A. System and the model

We consider a 1D array of circuit QED systems (see Fig. 1). Each cQED consists of the resonator, a superconducting microwave transmission line, and the qubit, a superconducting quantum bit (two-level system).<sup>9,24</sup> It is theoretically described by the Rabi Hamiltonian

$$H_i^{\text{cQED}} = \omega_0 a_i^\dagger a_i - \lambda (a_i + a_i^\dagger) \sigma_i^x + \frac{\Omega}{2} \sigma_i^z, \quad (1)$$

where  $a_i$  and  $a_i^\dagger$  are the field operators of the resonator with frequency  $\omega_0$ ,  $\sigma_i^x$  and  $\sigma_i^z$  are Pauli operators of the qubit with energy splitting  $\Omega$ , and  $\lambda$  the resonator-qubit coupling energy in the  $i$ th cQED.

The resonators of neighboring cQEDs are coupled capacitively to each other, and the microwave photons can hop from one resonator to nearby ones. Such hopping of microwave photons from resonator  $i$  to  $i + 1$  is described by the Hamiltonian

$$H_i^{\text{hopping}} = -J (a_i^\dagger a_{i+1} + a_{i+1}^\dagger a_i), \quad (2)$$

where  $J$  is the photon hopping amplitude. The Hamiltonian of the whole chain is then given by

$$H = \sum_{i=1}^N H_i^{\text{cQED}} + \sum_{i=1}^{N-1} H_i^{\text{hopping}}, \quad (3)$$

where  $N$  is the number of cQEDs in the chain.

If the onsite coupling energy  $\lambda$  is sufficiently smaller than  $\omega_0$ , then the counter-rotating terms in (1),  $a_i \sigma_i^- + a_i^\dagger \sigma_i^+$ , can be neglected within the spirit of the usual rotating-wave approximation. In this case, the cQED Hamiltonian reduces to the Jaynes-Cummings Hamiltonian, and Eq. (3) to the Jaynes-Cummings-Hubbard model, which exhibits the superfluid–Mott-insulator phase transition.<sup>3–6</sup> If, however,  $\lambda$  is comparable to  $\omega_0$  (the ultrastrong-coupling regime), the rotating-wave approximation can not be justified, and the Jaynes-Cummings-Hubbard model does not properly describe the arrays of cQEDs any longer. In the following sections, we investigate the consequences of the counter-rotating terms in the cQED arrays.

### B. A single circuit QED system in the ultrastrong-coupling regime

We begin our analysis by discussing the properties of a single cQED in the ultrastrong-coupling regime ( $\lambda \gtrsim \omega_0$ ). It is a building block for the cQED arrays, and it is crucial to first understand the low-lying states of a single cQED Hamiltonian before examining the low-energy excitations of the arrays. Unlike the Jaynes-Cummings Hamiltonian, the total number of excitations  $N = a_i^\dagger a_i + (\sigma_i^z + 1)/2$ , is not a good quantum number, but only is the even-odd parity of  $N$ . In other words,

the Hamiltonian (1) commutes with the “parity” operator

$$\Pi_i = \exp(-i\pi a_i^\dagger a_i) \sigma_i^z. \quad (4)$$

Hence, the Hilbert space  $\mathcal{E}$  is decomposed into two orthogonal subspaces  $\mathcal{E}_i^\pm$  of  $\pm$  parity  $\mathcal{E} = \mathcal{E}^+ \oplus \mathcal{E}^-$ , and correspondingly the Hamiltonian (1) into  $H_i^{\text{cQED}} = H_i^+ \oplus H_i^-$  with  $H_i^\pm$  residing on  $\mathcal{E}^\pm$ , respectively. This parity symmetry proves to be useful to investigate the energy levels and find the approximate expression for the low-lying states as shown in the following.<sup>19</sup>

Within each subspace  $\mathcal{E}_i^\pm$ , the Hamiltonian  $H_i^\pm$  can be described in effect by a single bosonic operator  $b_i = a_i \sigma_i^x$ : namely,

$$H_i^\pm = H_i^0 \pm H_i^1 \quad (5)$$

with

$$H_i^0 = \omega_0 (b_i^\dagger - \lambda/\omega_0)(b_i - \lambda/\omega_0), \quad (6)$$

where we have added a constant  $\lambda^2/\omega_0$ , and

$$H_i^1 = \frac{\Omega}{2} \cos(\pi b_i^\dagger b_i). \quad (7)$$

$H_i^0$  is simply a displaced harmonic oscillator and the ground state is a coherent state with an amplitude  $\lambda/\omega_0$ :

$$|\lambda/\omega_0\rangle_{b_i}^\pm = e^{-\lambda^2/2\omega_0^2} \sum_{n=0}^{\infty} \frac{(\lambda/\omega_0)^n}{\sqrt{n!}} |n\rangle_{b_i}^\pm. \quad (8)$$

Here,  $|n\rangle_{b_i}^\pm$  is a Fock basis for the bosonic mode  $b_i$  defined in the subspace  $\mathcal{E}_i^\pm$ , respectively. For  $\lambda/\omega_0 \gg 1$  (regardless of  $\Omega$ ), the term  $H_i^1$  can be treated perturbatively and shifts the energies of  $|\lambda/\omega_0\rangle_{b_i}^\pm$  relatively by an exponentially small amount,

$$\Delta \equiv \frac{\Omega}{2} \exp[-2(\lambda/\omega_0)^2] \quad (\ll \omega_0). \quad (9)$$

As one can see from the energy-level diagram in Fig. 2(a), the two nearly degenerate ground states  $|\lambda/\omega_0\rangle_{b_i}^\pm$  with an exponentially small energy splitting  $2\Delta$  are separated far (i.e., by  $\omega_0$ ) from higher levels. Therefore, we can safely confine ourselves within the ground-state subspace, in which the Hamiltonian (1) is reduced to

$$H_i^{\text{cQED}} = -\Delta \tau_i^z. \quad (10)$$

Here, we have introduced the pseudospin operator

$$\tau_i^z \equiv |\uparrow\rangle_i \langle \uparrow| - |\downarrow\rangle_i \langle \downarrow| \quad (11)$$

and taken simplified notations  $|\uparrow\rangle_i \equiv |\lambda/\omega_0\rangle_{b_i}^-$  and  $|\downarrow\rangle_i \equiv |\lambda/\omega_0\rangle_{b_i}^+$ .

In passing, for later discussion, we also note an interesting property of the ground states. Back in the  $\{a_i, \sigma_i^z\}$  basis, the nearly degenerate ground states are expressed as<sup>19,21</sup>

$$|\uparrow\rangle_i = \frac{|\lambda/\omega_0\rangle_i |+\rangle_i - |-\lambda/\omega_0\rangle_i |-\rangle_i}{\sqrt{2}}, \quad (12a)$$

$$|\downarrow\rangle_i = \frac{|\lambda/\omega_0\rangle_i |+\rangle_i + |-\lambda/\omega_0\rangle_i |-\rangle_i}{\sqrt{2}}, \quad (12b)$$

where  $|\alpha\rangle_i$  ( $\alpha \in \mathbb{C}$ ) is the eigenstate (coherent state) of  $a_i$  and  $|\pm\rangle_i$  are the eigenstates of  $\sigma_i^x$  (see Table I). Clearly, these states have a high degree of entanglement between the resonator and

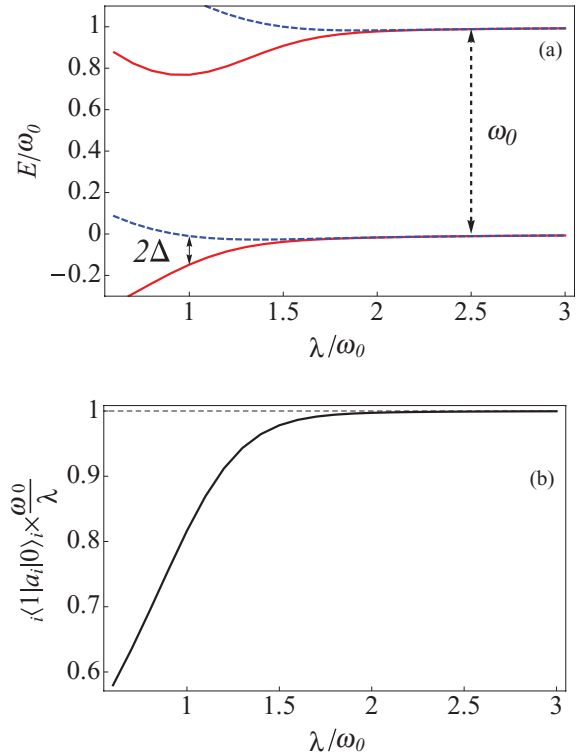


FIG. 2. (Color online) (a) Energy-level diagram for the circuit QED Hamiltonian (1) as a function of  $\lambda/\omega_0$ . Red (blue) curves are for even (odd) parity. (b) Plot of  $\frac{\omega_0}{\lambda} \langle \downarrow | a_i | \uparrow \rangle_i$ . We can conclude that  $\lambda > 2\omega_0$  is required for our model to be valid because the transverse field  $\Delta$  almost vanishes and the identification of photon annihilation operator as a spin-flip operator  $\frac{\omega_0}{\lambda} a_i = \tau_i^x$  is justified.

the qubit within the cQED. Following, we will see that such entanglement is extended over the whole cQED chain.

### C. Photon hopping term: Mapping to the Ising interaction

Now, we examine the effects of photon hopping [ $H_i^{\text{hopping}}$  in Eq. (2)] on the two lowest levels of the cQED Hamiltonian, given in Eq. (12). The photon hopping amplitude  $J$  is determined by the capacitance between the resonators, and typically it is much smaller than the photon frequency, that is,  $J \ll \omega_0$ . As we have shown in the previous section,  $\omega_0$  determines the energy gap separating the states  $|\uparrow\rangle_i$  and  $|\downarrow\rangle_i$  from higher levels. Therefore, in the first-order approximation, we can project the photon hopping Hamiltonian (2) to the subspace spanned by the states  $|\uparrow\rangle_i$  and  $|\downarrow\rangle_i$ . Remarkably, there is a simple relation between the two states,

TABLE I. Notations for the qubit ( $\sigma_i^z$ ), the pseudospin ( $\tau_i^z$ ), and the macroscopic pseudospin  $S^z$  basis.

$\sigma_i^z$	$\sigma_i^x$	$\tau_i^z$	$\tau_i^x$	$S^z$	$S^x$
$ 0\rangle_i$	$ +\rangle_i$	$ \uparrow\rangle_i$	$ \rightarrow\rangle_i$	$ \uparrow\rangle$	$ \Rightarrow\rangle$
$ 1\rangle_i$	$ -\rangle_i$	$ \downarrow\rangle_i$	$ \leftarrow\rangle_i$	$ \downarrow\rangle$	$ \Leftarrow\rangle$
$ \pm\rangle_i = \frac{ 0\rangle_i \pm  1\rangle_i}{\sqrt{2}}$		$ \rightleftharpoons\rangle_i = \frac{ \uparrow\rangle_i \pm  \downarrow\rangle_i}{\sqrt{2}}$		$ \rightleftharpoons\rangle = \frac{ \uparrow\rangle \pm  \downarrow\rangle}{\sqrt{2}}$	

that is,

$$a_i |\uparrow\rangle_i = \lambda/\omega_0 |\downarrow\rangle_i, \quad (13)$$

$$a_i |\downarrow\rangle_i = \lambda/\omega_0 |\uparrow\rangle_i. \quad (14)$$

This is in stark contrast to the vacuum of the Jaynes-Cummings Hamiltonian, where applying the annihilation operator to the ground state leads to zero. It is a direct consequence of the peculiar structure of the vacuum of cQED Hamiltonian in the ultrastrong-coupling regime. As one can see in Eq. (12), the cavity part of the ground states consists of two coherent states with the same amplitude and opposite phases. Since the coherent state is the eigenstate of the annihilation operator  $a_i$ , it only changes relative phase between the two amplitudes. From this relation, we can map both the creation and annihilation operator to pseudo-spin-flip operator

$$a_i, a_i^\dagger \rightarrow \frac{\lambda}{\omega_0} (|\downarrow\rangle_i \langle\uparrow| + |\uparrow\rangle_i \langle\downarrow|) \equiv \frac{\lambda}{\omega_0} \tau_i^x. \quad (15)$$

In Fig. 2(b), the accuracy of this mapping is demonstrated. It turns out that the mapping is very accurate as long as  $\lambda \gtrsim 2\omega_0$ .

Finally, the photon hopping Hamiltonian can be mapped to the Ising interaction between the states  $|\uparrow\rangle_i$  and  $|\downarrow\rangle_i$ , that is,

$$H_i^{\text{hopping}} = -J_{\text{eff}} \tau_i^x \tau_{i+1}^x \quad (16)$$

with  $J_{\text{eff}} = 2J(\lambda/\omega_0)^2$ . The effective Ising interaction strength  $J_{\text{eff}}$  is renormalized with respect to  $J$  by the factor  $(\lambda/\omega_0)^2$  because the field part of the pseudospin states in Eq. (12) is a coherent state with amplitudes  $\lambda/\omega_0$  and the field-field interaction between resonators is proportional to the amplitudes of the resonator fields.

#### D. A transverse-field Ising chain

Let us now investigate the whole chain described by the Hamiltonian (3). As we have explained in Sec. II B, we can consider each cQED as a pseudospin. Thus, the circuit QED arrays can be regarded as a 1D spin chain

$$\sum_i^N H_i^{\text{cQED}} = -\Delta \sum_i^N \tau_i^z. \quad (17)$$

In addition, we have shown in Sec. II C that the photon hopping can be mapped to the Ising interaction between the nearest-neighborhood spins in the spin chain:

$$\sum_{i=1}^{N-1} H_i^{\text{hopping}} = -J_{\text{eff}} \sum_{i=1}^{N-1} \tau_i^z \tau_{i+1}^z. \quad (18)$$

Putting both (17) and (18) together into the total Hamiltonian (3), the low-energy effective Hamiltonian for the cQED chain becomes the so-called transverse-field Ising model (TFIM)

$$H_{\text{Ising}} = -\Delta \sum_i^N \tau_i^z - J_{\text{eff}} \sum_i^N \tau_i^x \tau_{i+1}^x. \quad (19)$$

The TFIM exhibits a quantum phase transition between the *magnetically ordered* phase for  $\Delta < J_{\text{eff}}$  and the *quantum paramagnet* phase for  $\Delta > J_{\text{eff}}$ .<sup>25</sup> The former is particularly interesting because it permits nearly degenerate ground states of the system. We will also see in Sec. III that it corresponds

to the topologically nontrivial phase in the Majorana chain. Interestingly, the ultrastrong can realize the magnetically ordered phase. This is because the transverse field  $\Delta = \frac{\Omega}{2} e^{-2(\lambda/\omega_0)^2}$  decreases exponentially as a function of the ratio  $\lambda/\omega_0$ , while the effective Ising interaction  $J_{\text{eff}} = 2J(\lambda/\omega_0)^2$  increases quadratically.

For  $\Delta = 0$ ,  $H_{\text{Ising}}$  has two degenerate ground states

$$|\Rightarrow\rangle \equiv \prod_i |\rightarrow\rangle_i, \quad |\Leftarrow\rangle \equiv \prod_i |\leftarrow\rangle_i, \quad (20)$$

where  $|\rightarrow\rangle_i$  and  $|\leftarrow\rangle_i$  are eigenstates of  $\tau_i^x$  (see Table I). For  $\Delta > 0$  (yet  $\Delta < J_{\text{eff}}$ ),  $\tau_i^z$  tends to flip the pseudospins  $|\rightarrow\rangle_i \leftrightarrow |\leftarrow\rangle_i$ . It causes tunneling between  $|\Rightarrow\rangle$  and  $|\Leftarrow\rangle$  via soliton propagation, and hence the true eigenstates become

$$|\Psi_0\rangle = \frac{1}{\sqrt{2}} (|\Rightarrow\rangle + |\Leftarrow\rangle), \quad |\Psi_1\rangle = \frac{1}{\sqrt{2}} (|\Rightarrow\rangle - |\Leftarrow\rangle). \quad (21)$$

However, as the tunneling involves  $N$  spins, the tunneling amplitude is exponentially suppressed with the system size  $N$ . In other words,  $|\Psi_0\rangle$  and  $|\Psi_1\rangle$  are nearly degenerate with energy splitting,  $\delta \sim \exp(-N/\xi)$  with  $\xi$  being the correlation length of the Ising chain, exponentially small in system size  $N$ . Both are separated from the continuum of excitations by the energy gap  $J_{\text{eff}}$ . Expressed in terms of pseudospins,  $|\Psi_0\rangle$  and  $|\Psi_1\rangle$  in Eq. (21) take the typical form of the GHZ state,<sup>26</sup> incorporating a high degree of nonlocal entanglement.

#### E. Large-scale maximal entanglement in the ground states

The ground states expressed in terms of the pseudospins in Eq. (21) allow us to find the ground-state wave function of the circuit QED arrays in terms of the cavity fields and the qubit states. First, the eigenstate of the  $\tau_x$  operator  $|\rightarrow\rangle$  is

$$|\rightarrow\rangle_i = |\uparrow\rangle_i + |\downarrow\rangle_i = |\lambda\rangle_i |+\rangle_i, \quad (22)$$

$$|\leftarrow\rangle_i = |\uparrow\rangle_i - |\downarrow\rangle_i = |-\lambda\rangle_i |-\rangle_i. \quad (23)$$

Then, the two degenerate ground states for  $\Delta = 0$  become

$$|\Rightarrow\rangle = \prod_{i=1}^N |\lambda/\omega_0\rangle_i |+\rangle_i, \quad |\Leftarrow\rangle = \prod_{i=1}^N |-\lambda/\omega_0\rangle_i |-\rangle_i. \quad (24)$$

That is,  $|\Rightarrow\rangle$  indicates that each of the cavity fields is displaced to the  $+x$  direction in the phase space with an amplitude determined by the ratio  $\lambda/\omega_0$ , while each of the qubits is directing the  $+x$  direction in the Bloch sphere. Similarly,  $|\Leftarrow\rangle$  indicates all the cavities are displaced to the  $-x$  direction, while qubits are directing the  $-x$  direction. Finally, the true eigenstates of the chain [Eq. (21)] are a superposition of these two macroscopically distinctive states,

$$|\Psi_s\rangle = \frac{1}{\sqrt{2}} \left[ \prod_i^N |\lambda/\omega_0\rangle_i |+\rangle_i + (-1)^s \prod_i^N |-\lambda/\omega_0\rangle_i |-\rangle_i \right] \quad (25)$$

with  $s = 0$  or  $1$ . The entanglement involves large-amplitude ( $\lambda/\omega_0 \gg 1$ ) coherent states of the cavity fields, and the scale to which they are entangled with the qubits is truly macroscopic in the sense that Eq. (25) is a superposition of two orthogonal states of fields and qubits distributed across

a chain of centimeter-long resonators. Entanglement over a fraction of a meter can be achievable even with a moderate number of resonators.

### III. A MAJORANA CHAIN

The 1D TFIM discussed above is equivalent to a chain of Majorana fermions.<sup>27,28</sup> The latter has attracted great interest because it permits localized Majorana modes that can be used for topologically protected quantum computation.<sup>27–29</sup> A very recent experiment<sup>30</sup> suggests that the Majorana chain can be realized in a solid-state system, and intensive efforts are made in this direction.<sup>31</sup>

Here, we reexpress the two nearly degenerate states in Eq. (21) or (25) in terms of localized Majorana fermions, and later discuss an experimentally feasible way of probing such Majorana fermions. The equivalence between the TFIM and the Majorana chain can be seen through a Jordan-Wigner transformation:<sup>32</sup>  $c_i^\dagger = \tau_i^+ \prod_{j=1}^{i-1} (-\tau_j^z)$  with  $\tau_i^+ = \frac{1}{2}(\tau_i^x + i\tau_i^y)$ . The operators  $c_i$  and  $c_i^\dagger$  describe Dirac fermions and satisfy  $\{c_i, c_j^\dagger\} = \delta_{ij}$  and  $\{c_i, c_j\} = 0$ . The Dirac fermion operators are further represented with self-conjugate Majorana operators  $\gamma_{2i-1} = c_i^\dagger + c_i$  and  $\gamma_{2i} = i(c_i^\dagger - c_i)$ . The TFIM (19) is then reduced to

$$H_{\text{Majorana}} = \frac{i}{2} \left[ \Delta \sum_{i=1}^N \gamma_{2i-1} \gamma_{2i} + J_{\text{eff}} \sum_i^{N-1} \gamma_{2i} \gamma_{2i+1} \right]. \quad (26)$$

At  $\Delta = 0$ , the Majoranas at the two ends,  $\gamma_1$  and  $\gamma_{2N}$ , in the chain do not appear in the Hamiltonian, which implies the existence of two degenerate ground states. These are nothing but  $|\Rightarrow\rangle$  and  $|\Leftarrow\rangle$  in Eq. (20). For finite  $\Delta$ , the two states  $|\Rightarrow\rangle$  and  $|\Leftarrow\rangle$  are mixed linearly into  $|\Psi_0\rangle$  and  $|\Psi_1\rangle$  in Eq. (25) due to the tunneling between two Majorana modes  $\gamma_1$  and  $\gamma_{2N}$ , and the degeneracy is lifted. Since the tunneling is through the whole chain, the energy splitting  $\delta$  is exponentially small (as long as  $\Delta < J_{\text{eff}}$ ). One can check that  $(\gamma_1 + i\gamma_{2N})|\Psi_0\rangle = 0$  and  $(\gamma_1 + i\gamma_{2N})|\Psi_1\rangle = 2|\Psi_0\rangle$ , which means that  $|\Psi_1\rangle$  has one more fermion than  $|\Psi_0\rangle$  or equivalently that  $|\Psi_0\rangle$  and  $|\Psi_1\rangle$  have different fermion parities.

Here, we emphasize that the two Majoranas localized at the ends of the Majorana chain are actually nonlocal in the physical chain, i.e., the cQED chain or the Ising chain.<sup>23</sup> The Majorana operators are represented in terms of  $\tau_j^x$  and  $\tau_j^z$  as

$$\gamma_1 = \tau_1^x, \quad \gamma_{2N} = i\tau_N^x \prod_{j=1}^N (-\tau_j^z), \quad (27)$$

and  $\gamma_{2N}$  involves the *string* operator  $\prod_{j=1}^N (-\tau_j^z)$ . This implies that the two nearly degenerate ground states  $|\Psi_0\rangle$  and  $|\Psi_1\rangle$  are not protected topologically against local noises even though mathematically they correspond to two distinct Majorana modes. It is contrary to the case where the two Majorana modes at the ends of a  $p$ -wave superconducting wire are topologically protected. However, we will see in the following that the Majorana bound states realized in cQED arrays can be indeed detected within the time scale that the noises destroy this exotic phase.

## IV. EFFECTS OF NOISES AND DISORDERS

### A. Noises

In this section, we examine the effects of the local noises on the coherence of the maximally entangled macroscopic ground states in Eq. (25) or, equivalently, on the Majorana bound states. The local noises induce fluctuation of the qubit parameters in  $\sigma_i^x$ ,  $\sigma_i^y$ , and  $\sigma_i^z$  directions, where  $\sigma_i^\mu$  indicates Pauli matrices for the *physical qubit* in the  $i$ th cavity. In addition, the intrinsic cavity decay will also affect the coherence of the quantum states. We model the environment using the baths of harmonic oscillators

$$H_b = \sum_{i=1}^N \sum_k \omega_{ik}^a c_{ik}^{a\dagger} c_{ik}^a + \sum_{q=x,y,z} \sum_{i=1}^N \sum_k \omega_{ik}^q c_{ik}^{q\dagger} c_{ik}^q, \quad (28)$$

where  $c_i^a$  is a bath operator for the  $i$ th cavity, and  $c_i^q$  a bath operator for the  $i$ th qubit in the  $q$  direction. The cQED array (system) described by Eq. (3) couples to the bath

$$H_{sb} = \sum_{i=1}^N \sum_k \kappa_{ik} (a_i + a_i^\dagger) (c_{ik}^a + c_{ik}^{a\dagger}) + \sum_{q=x,y,z} \sum_{i=1}^N \sum_k \gamma_{ik}^q \sigma_i^q (c_{ik}^q + c_{ik}^{q\dagger}), \quad (29)$$

where  $\kappa_{ik}$  is a cavity-bath coupling strength and  $\gamma_{ik}^q$  a qubit-bath coupling strength in the  $q$  direction. Our goal is to investigate the effects of baths on the lowest two levels of the system Hamiltonian in Eq. (25). Therefore, we first project the system Hamiltonian to the subspace spanned by  $|\Psi_{0,1}\rangle$ ,

$$H_s = \frac{\delta}{2} (|\Psi_1\rangle \langle \Psi_1| - |\Psi_0\rangle \langle \Psi_0|) \equiv -\frac{\delta}{2} S_z, \quad (30)$$

where  $\delta$  is the small energy splitting between  $|\Psi_{0,1}\rangle$ . By considering the system-bath coupling up to second order in  $\kappa_i$  and  $\gamma_i^q$ , we derive an effective spin-bath Hamiltonian (see Appendix A for details)

$$H_{sb}^{\text{eff}} = S_x \sum_{i=1}^N \left[ \sum_k \kappa_{ik} \frac{\lambda}{\omega_0} (c_{ik}^a + c_{ik}^{a\dagger}) + \sum_k \gamma_{ik}^x (c_{ik}^x + c_{ik}^{x\dagger}) - \frac{e^{-2\lambda^2/\omega_0^2}}{4J_{\text{eff}}} \times \sum_{q=y,z} \sum_{kl} (1 + \delta_{i1} + \delta_{iN}) \gamma_{ik}^q \gamma_{il}^q (2c_{ik}^{q\dagger} c_{il}^q + \delta_{kl}) \right]. \quad (31)$$

The first two terms are the first-order effects that come from  $a_i + a_i^\dagger$  and  $\sigma_i$ . From  $a_i |\Psi_{0(1)}\rangle = \lambda/\omega_0 |\Psi_{1(0)}\rangle$  and  $\sigma_i^x |\Psi_{0(1)}\rangle = |\Psi_{1(0)}\rangle$ , it is evident that these noises can depolarize the states in the first order. Interestingly, however, the structure of the wave function of  $|\Psi_{0,1}\rangle$  allows a partial protection against  $\sigma_y$  and  $\sigma_z$  noises. Note that

$$\langle \Psi_s | \sigma_i^{y,z} | \Psi_{s'} \rangle = 0 \quad (32)$$

with  $s, s' = 0, 1$ . Therefore, the noises along the  $\sigma_i^{y,z}$  directions can only affect the states from the second-order process. The third term in Eq. (31) comes from these noises. Not only is the second-order process energetically suppressed by the factor

$1/J_{\text{eff}}$ , which is the largest energy scale for the effective spin-bath system, but also there is an exponential suppression by the factor  $e^{-2\lambda^2/\omega_0^2}$ . The latter is reminiscent of the Franck-Condon effect and comes from the exponentially small overlap between the cavity states coupled to different qubit states in Eq. (25). By neglecting the second-order term and making the usual rotating-wave approximation for the system-bath coupling, the effective system-bath coupling Hamiltonian reads as

$$H_{sb}^{\text{eff}} = \sum_{i=1}^N (C_i^a + C_i^x) S_+ + \sum_{i=1}^N (C_i^{a\dagger} + C_i^{x\dagger}) S_- \quad (33)$$

with

$$C_i^a = \sum_k \kappa_{ik} \frac{\lambda}{\omega_0} c_{ik}^a, \quad C_i^x = \sum_k \gamma_{ik}^x c_{ik}^x \quad (34)$$

and  $S_{\pm} = (S_x \pm iS_y)$ . In Appendix B, we derive a master equation for the system density matrix using the above system-bath Hamiltonian, which has the standard form of the master equation

$$\dot{\rho}_s(t) = \Gamma \bar{n}(\delta, T) \mathcal{D}[S_+] \rho_s + \Gamma [\bar{n}(\delta, T) + 1] \mathcal{D}[S_-] \rho_s \quad (35)$$

with  $\mathcal{D}[O]\rho = \frac{1}{2}(2O\rho O^\dagger - \rho O^\dagger O - O^\dagger O\rho)$ . The rate is given by

$$\Gamma \equiv \sum_{i=1}^N \left( \frac{\lambda^2}{\omega_0^2} \Gamma_i^a + \Gamma_i^x \right), \quad (36)$$

where  $\Gamma_i^a$  is the cavity decay rate for the  $i$ th cavity and  $\Gamma^x$  is the decoherence rate for the  $i$ th physical qubit. Therefore, the decoherence rate for the  $|\Psi_{0,1}\rangle$  is nothing but a simple sum of decay rates and relaxation rates of the cavities and qubits, respectively, comprising the cQED arrays. Assuming that  $\Gamma_i^a = \Gamma^a$  and  $\Gamma_i^x = \Gamma^x$  for any  $i$ , the rate simply becomes  $N(\frac{\lambda^2}{\omega_0^2} \Gamma^a + \Gamma^x)$ . The decoherence rate is estimated to be  $\Gamma \sim 1$  MHz with  $N = 10$ , the intrinsic cavity decay rates  $\Gamma^a \sim 5$  kHz,<sup>33</sup> the qubit relaxation rate  $\Gamma^x \sim 100$  kHz,<sup>34</sup> and the ratio  $\lambda/\omega_0 \sim 2$ . In Sec. V, we propose a scheme to dispersively measure the states  $|\Psi_{0,1}\rangle$  using an additional cavity. The coupling strength between the states  $|\Psi_{0,1}\rangle$  and the additional cavity field is estimated to be much larger than the decoherence rate, indicating that the macroscopic ground states are measurable.

### B. Disorder

Due to imperfection in fabrication of the circuit QED arrays, inhomogeneity in system parameters is inevitable. The cavity frequency  $\omega_0$ , the qubit transition frequency  $\Omega$ , and the coupling strength  $\lambda$  can be different from one cQED to the other. The photon hopping amplitude  $J$  also can vary from site to site. For our effective spin Hamiltonian in Eq. (17), the inhomogeneity leads to site-dependent transverse-field strength and Ising interaction, that is, an inhomogeneous transverse-field Ising model

$$H_{\text{Ising}}^{\text{inhomo}} = - \sum_i \Delta_i \tau_i^z - \sum_i J_i^{\text{eff}} \tau_i^x \tau_{i+1}^x. \quad (37)$$

We note that the inhomogeneous Hamiltonian conserves the parity symmetry

$$[H_{\text{Ising}}^{\text{inhomo}}, P] = 0 \quad (38)$$

with

$$\mathcal{P} = \prod_{i=1}^N \tau_z^i. \quad (39)$$

Moreover, the states  $|\Psi_{1(0)}\rangle$  also have well-defined parity. Therefore, the ground states will be robust to small fluctuations in  $\Delta_i$  and  $J_i$ . We thus conclude that the macroscopic ground states  $|\Psi_0\rangle$  and  $|\Psi_1\rangle$  can be kept well protected by a careful design of the physical qubits in the system.<sup>13</sup>

### V. DETECTION SCHEME

In this section, we suggest a scheme to measure the macroscopic ground states of the circuit QED arrays. It can be also interpreted as detecting the Majorana bound states. Our proposal consists only of an additional empty resonator coupled to the resonator at the end of the circuit QED chain (see Fig. 3). Consider a resonator with a frequency  $\omega_d$  capacitively coupled to  $N$ th cavity, so that we have

$$H_d = J_d (a_N^\dagger a_d + a_N a_d^\dagger) + \omega_d a_d^\dagger a_d, \quad (40)$$

where  $a_N$  represents the field operator of the  $N$ th cavity, and  $a_d$  the field operator of the detection cavity. As shown earlier, the  $N$ th cavity's creation and annihilation operators are equivalent to  $\lambda/\omega_0 \tau_N^x$  for the  $N$ th effective spin. Moreover, for the nonlocal spin qubits,  $\tau_i^x$  is equivalent to  $S^x = |\Psi_0\rangle \langle \Psi_1| + |\Psi_1\rangle \langle \Psi_0|$  for any  $i$  as  $\tau_i^x |\Psi_s\rangle = |\Psi_{1-s}\rangle$  ( $s = 0, 1$ ). Therefore, assuming that  $\tilde{J}_d \equiv J_d \lambda/\omega_0 \ll J_{\text{eff}}$ , the low-energy effective Hamiltonian (30) combined with the detection Hamiltonian (40) leads again to the Rabi Hamiltonian

$$H_{\text{Rabi}} = -\frac{\delta}{2} S^z + \tilde{J}_d S^x (a_d + a_d^\dagger) + \omega_d a_d^\dagger a_d. \quad (41)$$

Here, we can make the rotating-wave approximation, then the Hamiltonian reduces to the Jaynes-Cummings Hamiltonian. Therefore, by just adding an empty resonator at one end of the circuit QED array, we can realize a circuit QED Hamiltonian for the two levels  $|\Psi_{0,1}\rangle$ . It allows us to tap into the standard techniques available for the circuit QED to measure the macroscopic ground states. Moreover, the coupling strength

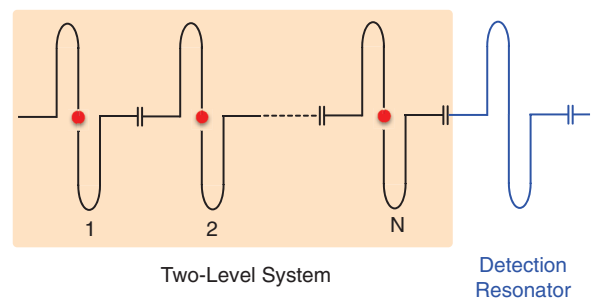


FIG. 3. (Color online) A detection scheme for the nearly degenerate ground states of the circuit QED arrays. The detection resonator is capacitively coupled to the  $N$ th resonator of the chain. This capacitive coupling leads to a coherent coupling between the nearly degenerate ground states and the detection resonator. In other words, the circuit QED arrays as a two-level system and the detection resonator as a cavity, the proposed setup realizes a circuit QED system. It allows the dispersive measurement of the two ground states by probing the detection resonator.

$J_d$  can have  $1 \sim 100$  MHz, while the decoherence rate for the macroscopic ground states is around 1 MHz as estimated in Sec. IV. Therefore, the detection circuit QED Hamiltonian in Eq. (41) realizes the strong-coupling regime. The effects of noises do destroy the coherence of the macroscopic ground states or the Majorana bound states, but they can be detected using the additional cavity within the coherence time of the states.

## VI. EXPERIMENTAL FEASIBILITY

Finally, we examine the experimental feasibility of the ideas explained above, estimating possible values of physical parameters of the system. Two requirements must be satisfied: First, the two ground states of each cQED in the system must be nearly degenerate and well separated from higher excitations. In Fig. 2(a) are plotted the energies of individual circuit QED Hamiltonian (1) in the resonant case ( $\omega_0 = \Omega$ ). Figure 2(b) plots  $\frac{\omega_0}{\lambda} \langle \downarrow | a_i | \uparrow \rangle_i$  to illustrate how good (its value close to 1) the approximation  $a_i = \lambda/\omega_0 \tau_i^x$  is. One can see that  $\lambda \sim 2\omega_0$  suffices for the requirement. Second, the system should be in the magnetically ordered phase (in terms of the effective TFIM)  $\Delta < J_{\text{eff}}$  or equivalently  $\Omega \exp[-2(\lambda/\omega_0)^2] < 4J(\lambda/\omega_0)^2$ . This requirement is satisfied provided that  $J > 10^{-5}\omega_0$ . The desired coupling strength  $\lambda > 2\omega_0$  seems achievable for the fluxonium coupled inductively to the superconducting resonator.<sup>21</sup> Moreover,  $J > 10^{-5}\omega_0$  is also realistic for the superconducting resonators, with  $J$  in the range of a few MHz.

## VII. CONCLUSION

We have found several intriguing properties of the two nearly degenerate ground states of a chain of coupled circuit QED systems in the ultrastrong-coupling regime. These ground states show maximal entanglement between macroscopic quantum states of radiation fields and states of qubits over a large scale, and are mathematically equivalent to Majorana bound states. By attaching an additional cavity to the arrays, one may realize a circuit QED Hamiltonian between the nearly degenerate ground states and the additional cavity, as well as achieve the strong-coupling regime. It would allow one to detect the ground states, equivalent to the Majorana bound states.

*Note added.* Recently, we have noticed a closely related papers.<sup>35</sup> While they focus on the phase transition of the circuit QED chain, we are mainly concerned about the quantum properties of the nearly degenerated ground states on one side of the phase transition. In this respect, both works are complementary to each other.

## ACKNOWLEDGMENT

This work has been supported by the NRF Grants (No. 2011-0012494 and No. 2010-0025880) and the 2nd stage BK21 Program.

## APPENDIX A: EFFECTIVE SYSTEM-BATH HAMILTONIAN

In this appendix, we derive the effective system-bath Hamiltonian given in Eq. (31) using the second-order perturbation

theory. From the system-bath Hamiltonian in Eq. (29), we first examine the terms with  $a_i + a_i^\dagger$  and  $\sigma_i^x$ ,

$$H_{sb}^{(1)} = \sum_{i=1}^N \sum_k \kappa_{ik} (a_i + a_i^\dagger) (c_{ik}^a + c_{ik}^{a\dagger}) + \sum_{i=1}^N \sum_k \gamma_{ik}^x \sigma_i^x (c_{ik}^x + c_{ik}^{x\dagger}). \quad (\text{A1})$$

The matrix elements are

$$\begin{aligned} \langle \Psi_0 | H_{sb}^{(1)} | \Psi_0 \rangle &= \langle \Psi_1 | H_{sb}^{(1)} | \Psi_1 \rangle = 0, \\ \langle \Psi_0 | H_{sb}^{(1)} | \Psi_1 \rangle &= \langle \Psi_1 | H_{sb}^{(1)} | \Psi_0 \rangle \\ &= \sum_{i=1}^N \sum_k \left( \kappa_{ik} \frac{\lambda}{\omega_0} (c_{ik}^a + c_{ik}^{a\dagger}) + \gamma_{ik}^x (c_{ik}^x + c_{ik}^{x\dagger}) \right). \end{aligned} \quad (\text{A2})$$

Therefore, the terms with  $a_i + a_i^\dagger$  and  $\sigma_i^x$  can depolarize the two levels  $S_z$  in the first order in  $\kappa_i$  and  $\gamma_i^x$ :

$$H_{sb}^{(1)} = S_x \left[ \sum_{i=1}^N \sum_k \kappa_{ik} \frac{\lambda}{\omega_0} (c_{ik}^a + c_{ik}^{a\dagger}) + \sum_{i=1}^N \sum_k \gamma_{ik}^x (c_{ik}^x + c_{ik}^{x\dagger}) \right]. \quad (\text{A3})$$

Note that the  $\lambda/\omega_0$  factor comes from the amplitude of the coherent states in  $|\Psi_{0,1}\rangle$ . Now, we look at the terms with  $\sigma_i^y$  and  $\sigma_i^z$ :

$$H_{sb}^{(2)} = \sum_{q=y,z} \sum_{i=1}^N \sum_k \gamma_{ik}^q \sigma_i^q (c_{ik}^q + c_{ik}^{q\dagger}). \quad (\text{A4})$$

As noted earlier, the first-order contribution from these noise sources vanishes  $\langle \Psi_s | \sigma_i^{y,z} | \Psi_{s'} \rangle = 0$  with  $s, s' = 0, 1$ . Although the exact formula for the second-order perturbation requires knowledge of the eigenfunctions for excited states, we can estimate the order of magnitude by considering the elementary excitations. For the transverse-field Ising model with a ferromagnetic coupling, the elementary excitations that can be excited from the magnetically ordered ground states are those that flip  $m$ th pseudospin from the ordered states in Eq. (24), that is,

$$\begin{aligned} |\Psi_m^{e+}\rangle &= |-\lambda/\omega_0\rangle_m |-\rangle_m \prod_{i \neq m} |\lambda/\omega_0\rangle_i |+\rangle_i, \\ |\Psi_m^{e-}\rangle &= |\lambda/\omega_0\rangle_m |+\rangle_m \prod_{i \neq m} |-\lambda/\omega_0\rangle_i |-\rangle_i \end{aligned} \quad (\text{A5})$$

with all of the energy is approximately above  $4J_{\text{eff}}$  from the ground states, except for  $m = 1, N$  whose energy is above  $2J_{\text{eff}}$ . The transition matrix then reads as

$$\sum_{m=1}^N \sum_{p=\pm} (1 + \delta_{m1} + \delta_{mN}) \frac{\langle \Psi_s | H_{sb}^{(2)} | \Psi_m^{ep} \rangle \langle \Psi_m^{ep} | H_{sb}^{(2)} | \Psi_{s'} \rangle}{4J_{\text{eff}}}. \quad (\text{A6})$$

To calculate this, we first make the rotating-wave approximation on  $H_{sb}^{(2)}$ , and define the lowering and raising operators for the  $x$ -direction spin  $\sigma_i^{x\pm} = \frac{1}{2}(\sigma_i^z \mp i\sigma_i^y)$ .

The act of the operators on the ground states leads to

$$\sigma_n^{x+} |\Psi_s\rangle = (-1)^s |\lambda/\omega_0\rangle_n |+\rangle_n \prod_{i \neq n}^N |\lambda/\omega_0\rangle_i |-\rangle_i, \quad (\text{A7})$$

$$\sigma_n^{x-} |\Psi_s\rangle = |\lambda/\omega_0\rangle_n |-\rangle_n \prod_{i \neq n}^N |\lambda/\omega_0\rangle_i |+\rangle_i, \quad (\text{A8})$$

which then leads to

$$\langle \Psi_m^{e-} | \sigma_n^{x+} | \Psi_s \rangle = \delta_{nm} (-1)^s e^{-2\lambda^2/\omega_0^2}, \quad (\text{A9})$$

$$\langle \Psi_m^{e+} | \sigma_n^{x-} | \Psi_s \rangle = \delta_{nm} e^{-2\lambda^2/\omega_0^2}. \quad (\text{A10})$$

The exponential factor  $e^{-2\lambda^2/\omega_0^2}$  is an overlap between coherent states with an amplitude  $\lambda/\omega_0$  and opposite phases. From this, we obtain the second-order system-bath Hamiltonian

$$H_{sb}^{\text{eff},2} = (S_0 - S_x) \frac{e^{-4\lambda^2/\omega_0^2}}{4J_{\text{eff}}} \sum_{q=y,z} \sum_{i=1}^N \sum_{kl} (1 + \delta_{i1} + \delta_{iN}) \times \gamma_{ik}^q \gamma_{il}^q (2b_{ik}^{q\dagger} b_{il}^q + \delta_{kl}). \quad (\text{A11})$$

After neglecting the identity term  $S_0$  and combined with the first-order term, we have arrived at Eq. (31).

## APPENDIX B: MASTER EQUATION

In this section, we derive the master equation in Eq. (35) starting from the effective system-bath coupling Hamiltonian in Eq. (33). We note that the bath correlation function for  $C \equiv \sum_i C_i^a + C_i^x$  is a sum of the correlation function for each bath operator, that is,

$$\begin{aligned} \langle C^\dagger(t) C(t') \rangle &= \sum_{i=1}^N \langle C_i^{a\dagger}(t) C_i^a(t') \rangle + \sum_{i=1}^N \langle C_i^{x\dagger}(t) C_i^x(t') \rangle \\ &= \sum_{i=1}^N \sum_k \kappa_{ik}^2 \frac{\lambda^2}{\omega_0^2} e^{i\omega_{ik}^a(t-t')} \bar{n}(\omega_{ik}^a, T) \\ &\quad + \sum_{i=1}^N \sum_k \gamma_{ik}^2 e^{i\omega_{ik}^x(t-t')} \bar{n}(\omega_{ik}^x, T), \end{aligned} \quad (\text{B1})$$

where  $\bar{n}(\omega_{ik}^{a(x)}, T)$  is an average occupation number for the bath in the thermal equilibrium. Likewise, we have

$$\begin{aligned} \langle C(t) C^\dagger(t') \rangle &= \sum_{i=1}^N \sum_k \kappa_{ik}^2 \frac{\lambda^2}{\omega_0^2} e^{-i\omega_{ik}^a(t-t')} [\bar{n}(\omega_{ik}^a, T) + 1] \\ &\quad + \sum_{i=1}^N \sum_k \gamma_{ik}^2 e^{-i\omega_{ik}^x(t-t')} [\bar{n}(\omega_{ik}^x, T) + 1]. \end{aligned} \quad (\text{B2})$$

The Born-Markov master equation involves a time integral of the bath correlation functions

$$\int_0^\infty d\tau e^{-i\delta\tau} \langle C^\dagger(t) C(t-\tau) \rangle = \frac{\bar{n}(\delta, T)}{2} \sum_{i=1}^N \left( \frac{\lambda^2}{\omega_0^2} \Gamma_i^a + \Gamma_i^x \right) \quad (\text{B3})$$

and

$$\begin{aligned} \int_0^\infty d\tau e^{-i\delta\tau} \langle C(t) C^\dagger(t-\tau) \rangle \\ = \frac{\bar{n}(\delta, T) + 1}{2} \sum_{i=1}^N \left( \frac{\lambda^2}{\omega_0^2} \Gamma_i^a + \Gamma_i^x \right), \end{aligned} \quad (\text{B4})$$

where  $\delta$  is the energy splitting between  $|\Psi_{0,1}\rangle$ ,  $\tau = t - t'$  and the rates are defined as follows:

$$\Gamma_i^x = 2\pi g_i^x(\delta) [\gamma_i^x(\delta)]^2, \quad (\text{B5})$$

$$\Gamma_i^a = 2\pi g_i^a(\delta) [\kappa_i(\delta)]^2 \quad (\text{B6})$$

with  $g_i^{x,a}$  being the density of states of each bath. We have neglected terms corresponding to the Lamb shift. Finally, we arrive at the master equation in the Lindblad form

$$\begin{aligned} \dot{\rho}_s(t) &= \frac{\Gamma}{2} \bar{n}(\delta, T) [2S_+ \rho_s(t) S_- - S_- S_+ \rho_s(t) - \rho_s(t) S_- S_+] \\ &\quad + \frac{\Gamma}{2} [\bar{n}(\delta, T) + 1] [2S_- \rho_s(t) S_+ - S_+ S_- \rho_s(t) \\ &\quad - \rho_s(t) S_+ S_-]. \end{aligned} \quad (\text{B7})$$

\*choims@korea.ac.kr

<sup>1</sup>I. Bloch, J. Dalibard, and S. Nascimbène, *Nat. Phys.* **8**, 267 (2012).

<sup>2</sup>R. P. Feynman, *Int. J. Theor. Phys.* **21**, 467 (1982).

<sup>3</sup>M. J. Hartmann, F. G. S. L. Brandão, and M. B. Plenio, *Nat. Phys.* **2**, 849 (2006).

<sup>4</sup>A. D. Greentree, C. Tahan, J. H. Cole, and L. C. L. Hollenberg, *Nat. Phys.* **2**, 856 (2006).

<sup>5</sup>D. G. Angelakis, M. F. Santos, and S. Bose, *Phys. Rev. A* **76**, 031805 (2007).

<sup>6</sup>D. Rossini and R. Fazio, *Phys. Rev. Lett.* **99**, 186401 (2007); E. K. Irish, C. D. Ogden, and M. S. Kim, *Phys. Rev. A* **77**, 033801 (2008); M. I. Makin, J. H. Cole, C. Tahan, L. C. L. Hollenberg, and A. D. Greentree, *ibid.* **77**, 053819 (2008); J. Koch and K. Le Hur, *ibid.* **80**, 023811 (2009); S. Schmidt and G. Blatter, *Phys. Rev. Lett.* **103**, 086403 (2009); **104**, 216402 (2010).

<sup>7</sup>M. J. Hartmann, F. G. S. L. Brandão, and M. B. Plenio, *Phys. Rev. Lett.* **99**, 160501 (2007); A. Kay and D. G. Angelakis, *Europhys. Lett.* **84**, 20001 (2008); J. Cho, D. G. Angelakis, and S. Bose, *Phys. Rev. A* **78**, 062338 (2008).

<sup>8</sup>J. Cho, D. G. Angelakis, and S. Bose, *Phys. Rev. Lett.* **101**, 246809 (2008); I. Carusotto, D. Gerace, H. Tureci, S. De Liberato, C. Ciuti, and A. Imamoglu, *ibid.* **103**, 033601 (2009); J. Koch, A. A. Houck, K. L. Hur, and S. M. Girvin, *Phys. Rev. A* **82**, 043811 (2010).

<sup>9</sup>A. Wallraff, D. I. Schuster, A. Blais, L. Frunzio, R. S. Huang, J. Majer, S. Kumar, S. M. Girvin, and R. J. Schoelkopf, *Nature (London)* **431**, 162 (2004).

<sup>10</sup>R. J. Schoelkopf and S. M. Girvin, *Nature (London)* **451**, 664 (2008).

<sup>11</sup>T. Aoki, B. Dayan, E. Wilcut, W. P. Bowen, A. S. Parkins, T. J. Kippenberg, K. J. Vahala, and H. J. Kimble, *Nature (London)* **443**, 671 (2006).

- <sup>12</sup>K. Hennessy, A. Badolato, M. Winger, D. Gerace, M. Atatüre, S. Gulde, S. Fält, E. L. Hu, and A. Imamoglu, *Nature (London)* **445**, 896 (2007).
- <sup>13</sup>A. A. Houck, H. E. Türeci, and J. Koch, *Nat. Phys.* **8**, 292 (2012); D. L. Underwood, W. E. Shanks, J. Koch, and A. A. Houck, *Phys. Rev. A* **86**, 023837 (2012).
- <sup>14</sup>H. Wang, M. Mariantoni, R. C. Bialczak, M. Lenander, E. Lucero, M. Neeley, A. D. O'Connell, D. Sank, M. Weides, J. Wenner, T. Yamamoto, Y. Yin, J. Zhao, J. M. Martinis, and A. N. Cleland, *Phys. Rev. Lett.* **106**, 060401 (2011); M. Mariantoni, H. Wang, R. C. Bialczak, M. Lenander, E. Lucero, M. Neeley, A. D. O'Connell, D. Sank, M. Weides, J. Wenner, T. Yamamoto, Y. Yin, J. Zhao, J. M. Martinis, and A. N. Cleland, *Nat. Phys.* **7**, 287 (2011).
- <sup>15</sup>M. J. Hartmann, F. G. S. L. Brandão, and M. B. Plenio, *Laser Photon. Rev.* **2**, 527 (2008).
- <sup>16</sup>M. Devoret, S. Girvin, and R. Schoelkopf, *Ann. Phys. (NY)* **16**, 767 (2007); J. Bourassa, J. M. Gambetta, A. A. Abdumalikov, O. Astafiev, Y. Nakamura, and A. Blais, *Phys. Rev. A* **80**, 032109 (2009); J. Bourassa, F. Beaudoin, J. Gambetta, and A. Blais, *ibid.* **86**, 013814 (2012).
- <sup>17</sup>T. Niemczyk, F. Deppe, H. Huebl, E. P. Menzel, F. Hocke, M. J. Schwarz, J. J. Garcia-Ripoll, D. Zueco, T. Hümmer, E. Solano, A. Marx, and R. Gross, *Nat. Phys.* **6**, 772 (2010); P. Forn-Díaz, J. Lisenfeld, D. Marcos, J. J. García-Ripoll, E. Solano, C. J. P. M. Harmans, and J. E. Mooij, *Phys. Rev. Lett.* **105**, 237001 (2010); G. Günter, A. A. Anappara, J. Hees, A. Sell, G. Biasiol, L. Sorba, S. De Liberato, C. Ciuti, A. Tredicucci, A. Leitenstorfer, and R. Huber, *Nature (London)* **458**, 178 (2009).
- <sup>18</sup>S. Ashhab and F. Nori, *Phys. Rev. A* **81**, 042311 (2010).
- <sup>19</sup>M.-J. Hwang and M.-S. Choi, *Phys. Rev. A* **82**, 025802 (2010).
- <sup>20</sup>P. Nataf and C. Ciuti, *Phys. Rev. Lett.* **104**, 023601 (2010).
- <sup>21</sup>P. Nataf and C. Ciuti, *Phys. Rev. Lett.* **107**, 190402 (2011).
- <sup>22</sup>D. Braak, *Phys. Rev. Lett.* **107**, 100401 (2011); E. K. Irish *ibid.* **99**, 173601 (2007); J. Hausinger and M. Grifoni, *Phys. Rev. A* **82**, 062320 (2010); **83**, 030301 (2011); J. Casanova, G. Romero, I. Lizuain, J. J. García-Ripoll, and E. Solano, *Phys. Rev. Lett.* **105**, 263603 (2010); D. Zueco, G. Reuther, S. Kohler, and P. Hänggi, *Phys. Rev. A* **80**, 033846 (2009).
- <sup>23</sup>C.-E. Bardyn and A. Imamoglu, *Phys. Rev. Lett.* **109**, 253606 (2012).
- <sup>24</sup>A. Blais, R.-S. Huang, A. Wallraff, S. M. Girvin, and R. J. Schoelkopf, *Phys. Rev. A* **69**, 062320 (2004).
- <sup>25</sup>S. Sachdev, *Quantum Phase Transitions*, 2nd ed. (Cambridge University Press, Cambridge, UK, 2011).
- <sup>26</sup>D. M. Greenberger, M. A. Horne, and A. Zeilinger, in *Bell's Theorem, Quantum Theory, and Conceptions of the Universe*, edited by M. Kafatos (Kluwer Academic, Dordrecht, The Netherlands, 1989).
- <sup>27</sup>A. Kitaev, *Phys. Usp.* **44**, 131 (2001).
- <sup>28</sup>A. Kitaev and C. Laumann, [arXiv:0904.2771](https://arxiv.org/abs/0904.2771).
- <sup>29</sup>A. Kitaev, *Ann. Phys. (NY)* **321**, 2 (2006).
- <sup>30</sup>V. Mourik, K. Zuo, S. M. Frolov, S. R. Plissard, E. P. A. M. Bakkers, and L. P. Kouwenhoven, *Sci. Express* (to be published).
- <sup>31</sup>For a recent review, see J. Alicea, *Rep. Prog. Phys.* **75**, 076501 (2012).
- <sup>32</sup>E. Lieb, T. Schultz, and D. Mattis, *Ann. Phys. (NY)* **16**, 407 (1961).
- <sup>33</sup>L. Frunzio, A. Wallraff, D. Schuster, J. Majer, and R. Schoelkopf, *IEEE Trans. Appl. Supercond.* **15**, 860 (2005).
- <sup>34</sup>V. E. Manucharyan, N. A. Masluk, A. Kamal, J. Koch, L. I. Glazman, and M. H. Devoret, *Phys. Rev. B* **85**, 024521 (2012).
- <sup>35</sup>M. Schiró, M. Bordyuh, B. Öztop, and H. E. Türeci, *Phys. Rev. Lett.* **109**, 053601 (2012); H. Zheng and Y. Takada, *Phys. Rev. A* **84**, 043819 (2011).